Terbium Substituted Lanthanum Orthoniobate: Electrical and Structural Properties

Kacper Dzierzgowski[ID]**, Sebastian Wachowski**[ID]**, Maria Gazda and Aleksandra Mielewczyk-Gryń** *

Department of Solid State Physics, Faculty of Applied Physics and Mathematics, Gdańsk University of Technology, Narutowicza 11/12, 80-233 Gdańsk, Poland; kacper.dzierzgowski@pg.edu.pl (K.D.); sebastian.wachowski@pg.edu.pl (S.W.); maria.gazda@pg.edu.pl (M.G.)

* Correspondence: alegryn@pg.edu.pl; Tel.: +48-58-348-66-19

check for updates

Abstract: The results of electrical conductivity studies, structural measurements and thermogravimetric analysis of $La_{1-x}Tb_xNbO_{4+\delta}$ (x = 0.00, 0.05, 0.1, 0.15, 0.2, 0.3) are presented and discussed. The phase transition temperatures, measured by high-temperature x-ray diffraction, were 480 °C, 500 °C, and 530 °C for $La_{0.9}Tb_{0.1}NbO_{4+\delta}$, $La_{0.8}Tb_{0.2}NbO_{4+\delta}$, and $La_{0.7}Tb_{0.3}NbO_{4+\delta}$, respectively. The impedance spectroscopy results suggest mixed conductivity of oxygen ions and electron holes in dry conditions and protons in wet. The water uptake has been analyzed by the means of thermogravimetry revealing a small mass increase in the order of 0.002% upon hydration, which is similar to the one achieved for undoped lanthanum orthoniobate.

1. Introduction

Proton conducting ceramics have attracted much interest due to their possible applications in energy conversion, as protonic ceramic fuel cells (PCFC), proton ceramic electrolyzer cells (PCEC), hydrogen sensors, and chemical synthesis [1]. Among them, several distinctive groups can be listed: materials based on barium cerate–zirconate solid solutions [2], rare earth niobates [3,4], as well as other materials, e.g., calcium zirconate, rare earth tungstates, and lanthanum ytterbium oxide [5–8].

For the last decade, multiple rare earth orthoniobates systems have been investigated, with the interest being put on their electronic [9–11] along with ionic conduction with oxygen ions [9,10] and protons [3] as mobile charge carriers. Also, other interesting properties were observed in these materials, e.g., paramagnetism, ferroelectricity, and luminescent emission [1,12].

Lanthanum orthoniobate as a proton conductor has been widely investigated since 2006, when Hausgrud and Norby introduced 1 mol% calcium into the lanthanum sublattice as a way of enhancing protonic conductivity [13]. In the following years, multiple dopants have been introduced both into the lanthanum (e.g., by calcium [14], magnesium [15], or strontium [16–19]) and niobium (e.g., by vanadium [20–22], antimony [23–25], arsenic [26], or cobalt [27]) sublattices. Recently, we also reported the influence of co-doping, using praseodymium as a rare earth dopant and calcium as an acceptor dopant in the lanthanum sublattice, on these system properties [28]. The presence of a mixed 3+/4+ cation in the lanthanum sublattice leads to enhanced electronic conductivity and yielding a mixed proton-electron conductor. From the other point of view, such a substitution can affect not only conductivity but also the structure of the material. For example, as it has been reported for $Ce_{1-x}La_xNbO_{4+\delta}$, the increase of lanthanum content in the cerium sublattice caused a decrease in the phase transition temperature [29]. Following the cerium and praseodymium substitutions, a natural

next step was to introduce the third lanthanide with mixed valence—terbium. In this work, we present the structural and transport properties of terbium doped lanthanum orthoniobates. The influence of a dopant on the conductivity of the system has been determined by the means of electrochemical impedance spectroscopy and thermogravimetric analysis.

2. Experimental

Powders of $La_{1-x}Tb_xNbO_{4+\delta}$ (x = 0.00, 0.05, 0.1, 0.15, 0.2, 0.3) were prepared via the solid-state reaction route. La_2O_3 (99.99% Aldrich, preheated at 900 °C for 4 h), Tb_4O_7 (99.99% Aldrich), and Nb_2O_5 (99.99% Alfa Aesar, Haverhill, MA, USA) were used as starting materials. The stoichiometric amounts of the reagents were milled in an agate mortar in isopropanol. The obtained powders were uniaxially pressed at 400 MPa into 12 mm diameter pellets. The green bodies were calcined at 1000 °C for 12 h. After the first step of the synthesis, the specimens were ground into powders. In the second step, the powders were pressed again at 400 MPa and resintered at 1400 °C for 12 h.

The Powder X-Ray Diffraction (XRD) patterns were collected using Philips X'Pert Pro MPD with Cu Kα radiation. High-temperature XRD (HTXRD) analyses were carried out with an Anton Paar HTK-1200 high-temperature unit. XRD data were analyzed with the FullProf suite [30]. The density of the samples was determined by a vacuum-assisted Archimedes method. The liquid medium used for the measurements was kerosene. The samples were dried, soaked, and suspended in the medium prior to weighing. To enhance soaking, the samples were immersed in kerosene and placed under a vacuum in order to remove air from open pores.

The microstructure was characterized using FEI (Waltham, MA, USA) Quanta FEG 250 scanning electron microscope (SEM) equipped with EDAX Apollo-SD energy-dispersive X-ray spectroscopy (EDS) detector. The microstructure imaging was performed in High Vacuum mode with Everhart-Thornley detector working either in Secondary Electrons (SE) or Back-scattered Electrons (BSE) mode.

Thermogravimetric analysis (TGA) was performed using a Netzsch (Burlington, MA, USA) Jupiter® 449 F1. The as-prepared powders were heated to 1000 °C and held at this temperature for 0.5 h under dry air to remove water and possible surface carbon dioxide. The samples after dehydration were cooled to 300 °C in dry gas. After 2 h of stabilization, the dry purge gas was switched to the humidified gas (P_{H2O} = 0.023 atm), then after an additional 2 h, the purge gas was switched back to the dry gas.

Impedance spectroscopy measurements were performed to determine the electrical properties of the investigated materials. Impedance spectroscopy measurements were performed in the frequency range 1 Hz–1 MHz and 1 V amplitude on samples with ink painted platinum electrodes (ESL 5542). The measurements were performed in wet (2.4% H_2O) and dry technical air (20% O_2, 80% N_2) using Gamry Reference 3000 at the temperature range from 350 °C to 750 °C with 50 °C steps. Obtained data were analyzed with ZView software. Studies of conductivity as a function of pO_2 were performed within the range of 2×10^{-6} to 1 atm at 700 °C. Different values of pressure were obtained through mixing nitrogen (<2 ppm O_2) with oxygen (purity 99.999%) gas. Both dry and wet gases (2.4% H_2O) were used in the pO_2 -dependency study.

3. Results and Discussion

Figure 1 shows the X-ray diffractograms of the synthesized sample powders. All observed reflections were indexed within the monoclinic $LaNbO_4$ (ICSD 01-071-1405), therefore the samples may be regarded as single-phase orthoniobates. The Rietveld profile of the pattern and the difference plots for $La_{0.85}Tb_{0.15}NbO_{4+\delta}$ is presented in Figure 2b. The unit cell parameters of the compounds, refined with the Rietveld method, are listed in Table 1. Terbium substituting lanthanum (La^{3+} ionic radius for CN = 8 is 1.16 Å) can be present in the lattice as Tb^{3+} or Tb^{4+}. Ionic radii of Tb^{3+} or Tb^{4+} for CN = 8 are 1.04 Å and 0.88 Å, respectively [31]. The general trend of a decrease of the unit cell volume with increasing terbium content (Figure 2a) can be attributed to the lower ionic radius of terbium.
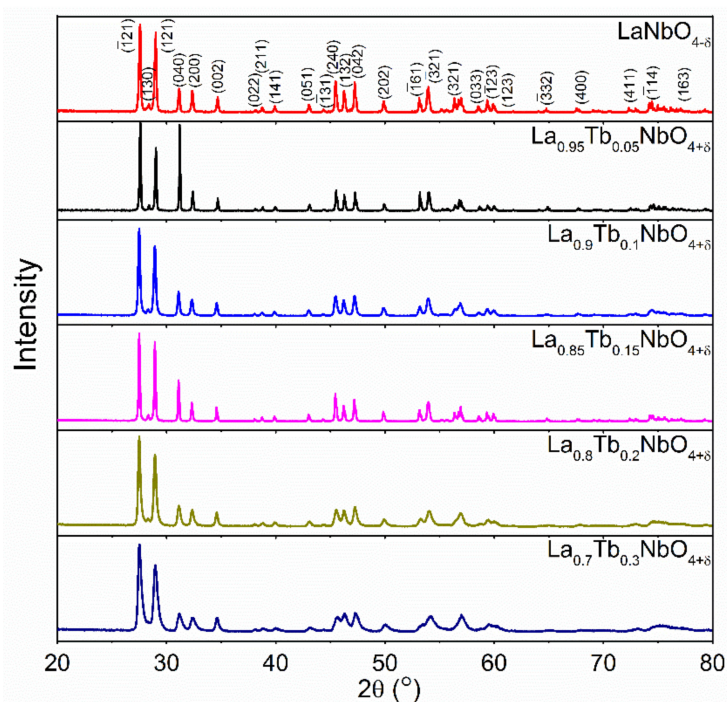
Figure 1. X-ray diffractograms of $La_{1-x}Tb_xNbO_{4+\delta}$ (x = 0.00, 0.05, 0.1, 0.15, 0.2, 0.3).

Table 1. Unit cell parameters and densities of $La_{1-x}Tb_xNbO_{4+\delta}$ (x = 0.00, 0.05, 0.1, 0.15, 0.2, 0.3); ϱ_t, ϱ_m, and ϱ_{rel} signify density calculated on the basis of unit cell parameters, density determined on the basis of Archimedes method, and relative density, respectively.

Sample	a (Å)	b (Å)	c (Å)	β (°)	V (Å³)	ϱ_t (g/cm³)	ϱ_m (g/cm³)	ϱ_{rel} (%)
$LaNbO_{4-\delta}$	5.5659	11.5245	5.2031	94.082	332.90	5.906	5.903	99.9
$La_{0.95}Tb_{0.05}NbO_{4+\delta}$	5.5509	11.4902	5.1954	94.091	330.52	5.963	5.214	87.5
$La_{0.9}Tb_{0.1}NbO_{4+\delta}$	5.5499	11.4934	5.1961	94.087	330.61	5.981	5.959	99.6
$La_{0.85}Tb_{0.15}NbO_{4+\delta}$	5.5532	11.4979	5.1969	94.092	330.97	5.995	5.259	87.7
$La_{0.8}Tb_{0.2}NbO_{4+\delta}$	5.5367	11.4648	5.1905	94.103	328.63	6.058	5.536	91.4
$La_{0.7}Tb_{0.3}NbO_{4+\delta}$	5.5202	11.4311	5.1812	94.103	326.11	6.145	5.525	89.9

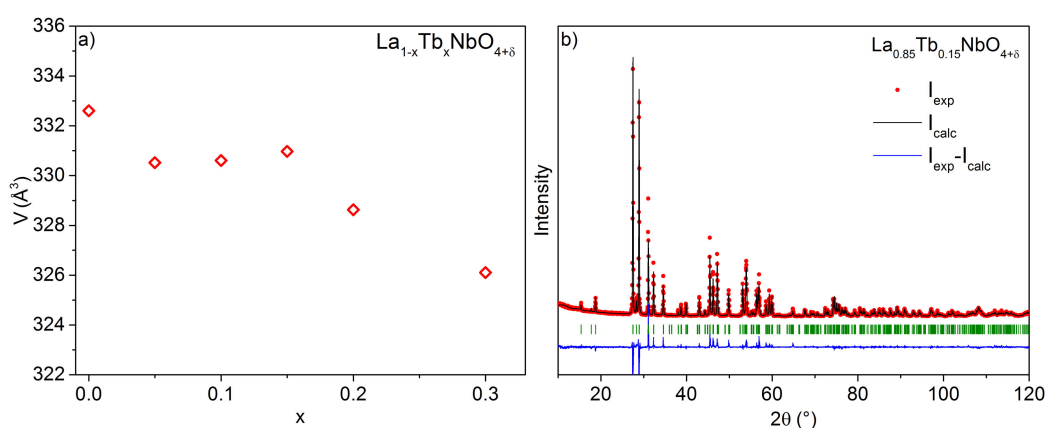**Figure 2.** (**a**) Unit cell volume as a function of Tb content in $La_{1-x}Tb_xNbO_{4+\delta}$. (**b**) The Rietveld profile of the pattern and the difference plots for $La_{0.85}Tb_{0.15}NbO_{4+\delta}$.

The XRD patterns of $La_{0.9}Tb_{0.1}NbO_{4+\delta}$ obtained between 460 °C and 490 °C are presented in Figure 3. It can be seen that the reflections corresponding to the $(\bar{1}21)$ and (121) planes of the monoclinic structure shift towards one another with increasing temperature and at 480 °C, they merge into one. This indicates the transition into the tetragonal phase. Similar behavior was observed in all studied samples. The phase transition temperatures were approximately 480 °C, 500 °C, and 530 °C for $La_{0.9}Tb_{0.1}NbO_{4+\delta}$, $La_{0.8}Tb_{0.2}NbO_{4+\delta}$, and $La_{0.7}Tb_{0.3}NbO_{4+\delta}$, respectively. Taking into consideration that terbium has a lower ionic radius than lanthanum, an increase of the transition temperature in $La_{1-x}Tb_xNbO_{4+\delta}$ with increasing terbium content is consistent with the other experimental results. For $RENbO_4$ with a decrease of rare earth metal ionic radius, an increase of phase transition temperature was observed [32].

Figure 4 shows exemplary SEM images taken of the sintered $La_{0.95}Tb_{0.05}NbO_{4+\delta}$, $La_{0.9}Tb_{0.1}NbO_{4+\delta}$, $La_{0.85}Tb_{0.15}NbO_{4+\delta}$, $La_{0.7}Tb_{0.3}NbO_{4+\delta}$ samples. In all samples, the observed fractures were apparently dense, without visible grain boundaries and with closed pores. Observed differences in porosity of the samples are consistent with the results of density measurements presented in Table 1. The relative densities vary from 87.5 ± 0.5 % ($La_{0.95}Tb_{0.05}NbO_{4+\delta}$) to 99.9 ± 0.3 % ($LaNbO_{4-\delta}$). The analysis performed with EDS and BSE detectors did not reveal secondary phases or impurities, which confirms the XRD results showing no phase separation.
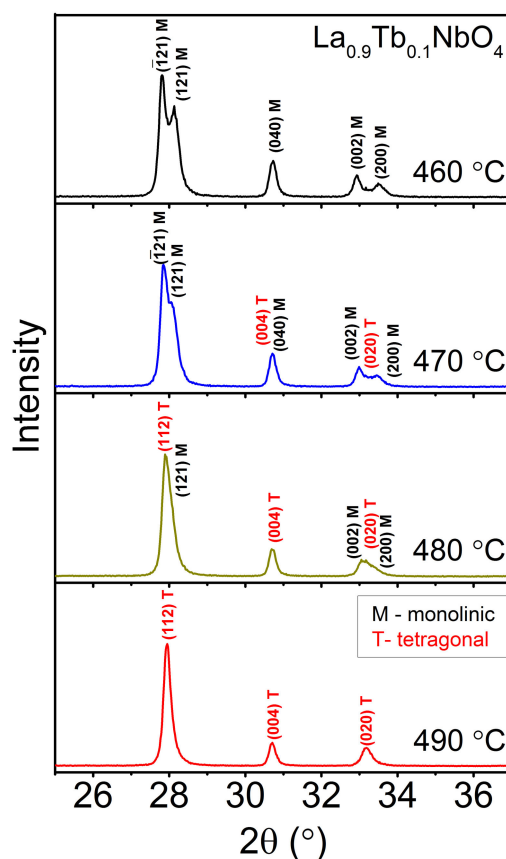

Figure 3. HTXRD patterns of $La_{0.9}Tb_{0.1}NbO_{4+\delta}$. Reflections of monoclinic and tetragonal phases were indexed with "M" and "T" letters, respectively.

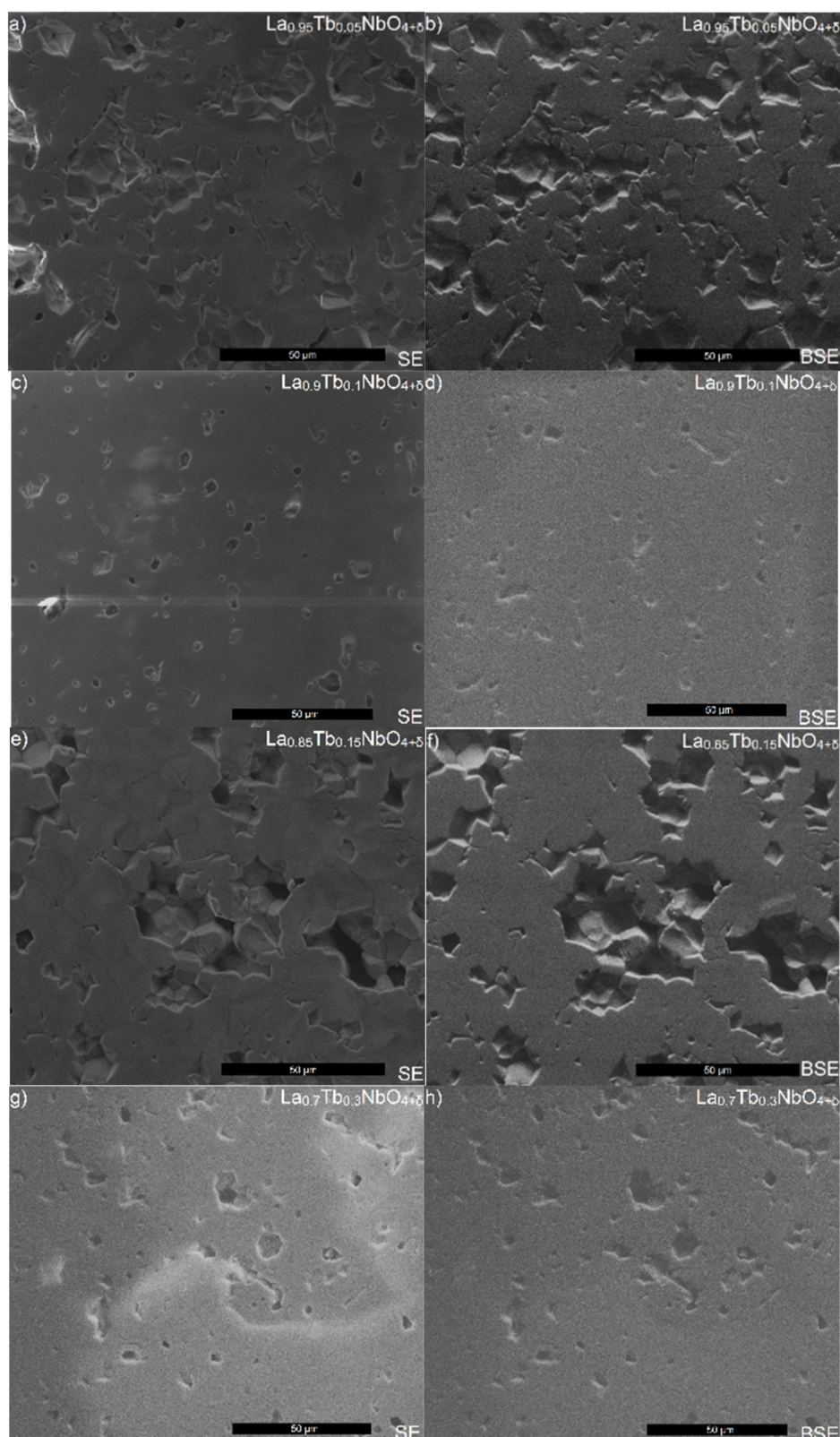**Figure 4.** SEM image of polished fractures of $La_{0.95}Tb_{0.05}NbO_{4+\delta}$, $La_{0.9}Tb_{0.1}NbO_{4+\delta}$, $La_{0.85}Tb_{0.15}NbO_{4+\delta}$, $La_{0.7}Tb_{0.3}NbO_{4+\delta}$ taken in SE and BSE mode.

Thermogravimetric analysis was performed in order to determine the water uptake of the investigated samples. The results obtained for $La_{0.9}Tb_{0.1}NbO_{4+\delta}$, $La_{0.8}Tb_{0.2}NbO_{4+\delta}$, and $La_{0.7}Tb_{0.3}NbO_{4+\delta}$ are presented in Figure 5. One can see that the weight change during gas switch is of the order of 0.002%.

This is much lower than the results reported by Yamazaki et al. for barium zirconate system, who at 300 °C obtained 0.5% [33]. However, this is in accordance with the results achieved for undoped lanthanum niobate [34]. The relatively small water uptake suggests a rather small concentration of the protons within the samples structures. In the view of a small proton concentration in lanthanum orthoniobates, it may be considered strange why the conductivity differences between wet and dry air reach 50–400% at 700 °C (Table 2). The most probable reason for that is relatively high mobility of protons as well as the absence of defect association phenomena. The proton mobility and trapping effects were discussed extensively by Huse et al. showing their importance in the process of conductivity in this system [35].
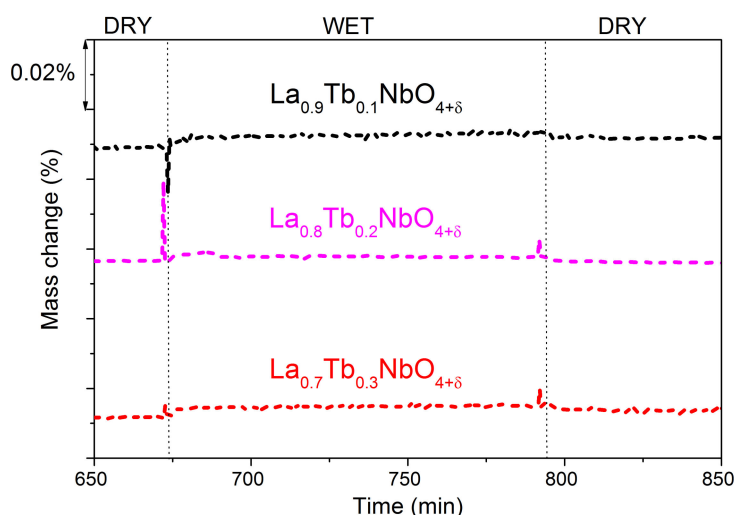

Figure 5. Results of TGA measurements performed for $La_{0.9}Tb_{0.1}NbO_{4+\delta}$, $La_{0.8}Tb_{0.2}NbO_{4+\delta}$, $La_{0.7}Tb_{0.3}NbO_{4+\delta}$.

Figure 6 presents an example of the acquired Nyquist plot for $La_{0.9}Tb_{0.1}NbO_{4+\delta}$. The clear curve separation into two semicircles can be seen. The brick layer model was used in the analysis of the impedance data [36]. The highest frequency semicircle is usually attributed to grain interior and the next semicircle is attributed to grain boundary conductivity [37]. Electrode responses, observed in the form of a low-frequency semicircle, as not in the scope of this study, were not analyzed. All impedance spectra were fitted with an equivalent circuit: $(CPE_g R_g)(CPE_{gb}R_{gb})$, where R is resistance and CPE is a constant phase element. For each semicircle, capacitances were calculated using the Formula (1).

$$C = Q_0^{\frac{1}{n}} R^{\frac{1}{n}-1} \tag{1}$$

where Q_0, the admittance and n, the angle of misalignment were calculated for each CPE. Typical values of capacitance obtained for high- and mid-frequency were 1×10^{-11} F/cm and 4×10^{-10} F/cm, respectively. The values are close to the ones typically observed in the literature [38] and confirm the semicircles were correctly attributed to grain, grain boundaries, and electrode processes. The conductivities of grain interior σ_g, specific grain boundary σ_{gb}, and total conductivity σ_{tot} were calculated with the use of Equations (2)–(4).

$$\sigma_g = S \frac{1}{R_g} \tag{2}$$

$$\sigma_{gb} = S \frac{1}{R_{gb}} \frac{C_g}{C_{gb}} \tag{3}$$

$$\sigma_{tot} = S \frac{1}{R_g + R_{gb}} \tag{4}$$

The *S* coefficient is a geometrical factor including sample porosity, thickness, and electrode area. Activation energies of total conductivity were calculated by fitting obtained values to the Equation (5), where σ is the conductivity, T is temperature, σ_0 is a pre-exponential factor, E_a is the activation energy, and k is the Boltzmann constant. Calculated values of activation energies are presented in Table 2.

Total conductivities of obtained samples in dry and wet air as a function of reciprocal temperature are presented in Figure 7. For all of the samples, the conductivity in wet air was higher than in dry air. The conductivity at 700 °C both in dry and wet air in the $La_{0.9}Tb_{0.1}NbO_{4+\delta}$ and $La_{0.85}Tb_{0.15}NbO_{4+\delta}$ samples reached 10^{-4} S/cm. Maximum conductivity at 700 °C was observed for the samples doped with 15% of terbium, while a further increase of Tb content led to the decline of total conductivity (Figure 8).

$$\sigma T = \sigma_0 e^{-\frac{E_a}{kT}} \tag{5}$$

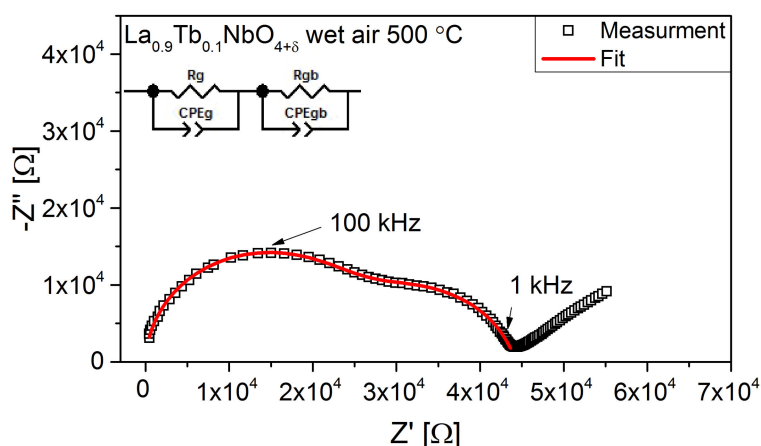

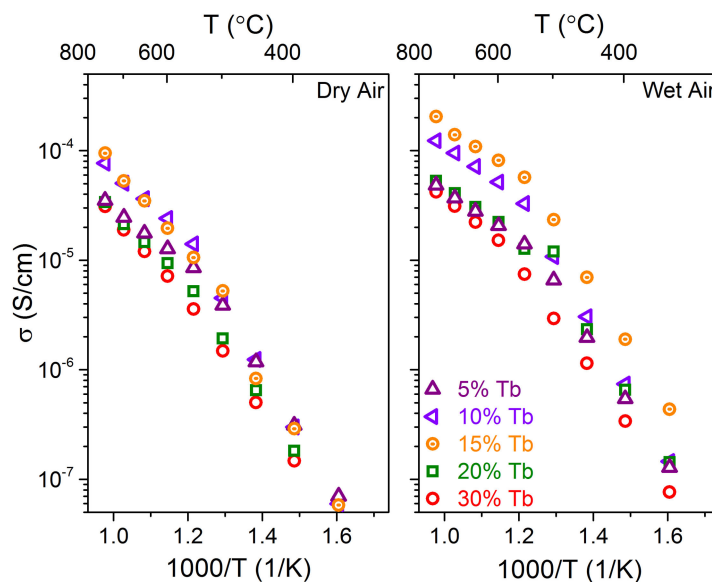**Figure 6.** Nyquist plot of $La_{0.9}Tb_{0.1}NbO_{4+\delta}$ measured in wet air at 500 °C.

Figure 7. Total conductivity as a function of the reciprocal temperature of $La_{1-x}Tb_xNbO_{4+\delta}$ in (**a**) dry air and (**b**) wet air.
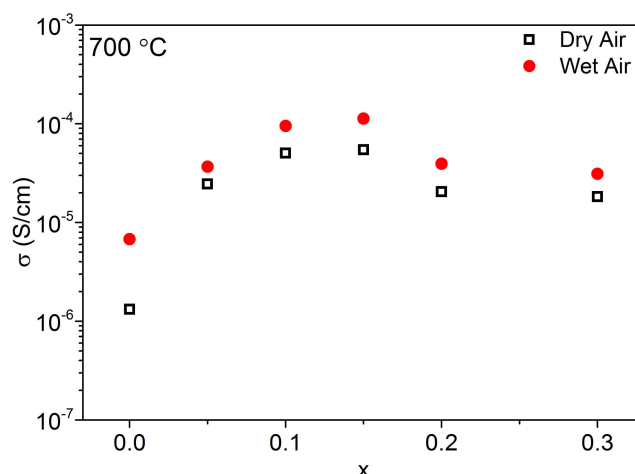
Figure 8. Total conductivities at 700 °C of $La_{1-x}Tb_xNbO_{4+\delta}$.

The change of slope of the plots observed at temperatures about 500 °C is related to the phase transition between the scheelite and fergusonite structures. Such behavior was observed before in many $LaNbO_{4-\delta}$-based materials [13,15,28,35]. The influence of the terbium content on the apparent activation energies of total conductivities (Table 2) is complex. In the low-temperature range, the values of activation energy in dry air decreases with the increase of Tb content. In the higher temperature range, the apparent activation energies are lower than these below 500 °C, however, no clear tendency of E_A dependence on Tb content can be observed. It should be noted that the $La_{0.8}Tb_{0.15}NbO_{4+\delta}$ sample, with the highest conductivities at 700 °C, shows also the lowest activation energies of conductivity in wet air, both for tetragonal (0.53 ± 0.02 eV) and monoclinic structure (1.16 ± 0.02 eV). Moreover, the strongest influence of humid atmosphere on the conductivity of this sample may be observed. The relative change of conductivity at 700 °C of $La_{0.8}Tb_{0.15}NbO_{4+\delta}$ reaches 107%, whereas in other doped materials, it is between 50 and 92%.

Table 2. Summary of electrical properties of $La_{1-x}Tb_xNbO_{4+\delta}$: total conductivities at 700 °C, a relative difference of total conductivities in wet and dry atmospheres at 700 °C, and apparent activation energies of conductivity in temperature ranges below and above 500 °C.

	σ_{tot}(700 °C)		$\frac{\sigma_{tot}^{wet}-\sigma_{tot}^{dry}}{\sigma_{tot}^{dry}}$	E_A Below 500 °C		E_A Above 500 °C	
	(10^{-5} S/cm)		(%)	(eV)		(eV)	
	Wet Air	**Dry Air**	**at 700 °C**	**Wet Air**	**Dry Air**	**Wet Air**	**Dry Air**
$LaNbO_{4-\delta}$	0.68	0.13	419	n/d	n/d	n/d	n/d
$La_{0.95}Tb_{0.05}NbO_{4+\delta}$	3.68	2.46	49	1.02 ± 0.02	1.29 ± 0.02	0.56 ± 0.02	0.68 ± 0.02
$La_{0.9}Tb_{0.1}NbO_{4+\delta}$	9.51	5.04	89	1.25 ± 0.02	1.25 ± 0.02	0.55 ± 0.02	0.68 ± 0.02
$La_{0.85}Tb_{0.15}NbO_{4+\delta}$	11.3	5.45	107	1.16 ± 0.02	1.24 ± 0.02	0.53 ± 0.02	0.86 ± 0.02
$La_{0.8}Tb_{0.2}NbO_{4+\delta}$	3.95	2.05	93	1.26 ± 0.02	1.11 ± 0.02	0.59 ± 0.02	0.74 ± 0.02
$La_{0.7}Tb_{0.3}NbO_{4+\delta}$	3.11	1.83	70	1.07 ± 0.03	1.15 ± 0.02	0.69 ± 0.05	0.85 ± 0.02

Figure 9 presents conductivity measured as a function of pO_2 in dry and wet atmospheres for $LaNbO_{4-\delta}$, $La_{0.05}Tb_{0.05}NbO_{4+\delta}$, and $La_{0.15}Tb_{0.85}NbO_{4+\delta}$. Under wet conditions, conductivity does not depend on oxygen partial pressure. Similarly, under dry conditions, the conductivity is almost independent for pO_2 below 10^{-4} atm, whilst above 10^{-3} atm it increases with increasing oxygen partial pressure. In terbium doped samples a stronger change of conductivity is observed, whereas in the $LaNbO_4$, change of conductivity is much smaller than in samples containing terbium. The observed slope of the conductivity at high pO_2 is close to $\frac{1}{4}$. Obtained results indicate that in wet conditions, materials are protonic conductors. In dry gases, the results show that at lower p_{O2}, the materials are oxygen ion conductors, whilst at high pO_2, the material is a mixed oxygen ion and electron holes conductor. The slope of the dependence observed in Figure 9 is characteristic of the situation where

ionic charge carriers have dominating concentration, whereas holes are a minority defect, but due to much higher mobility, contribute to total conductivity.
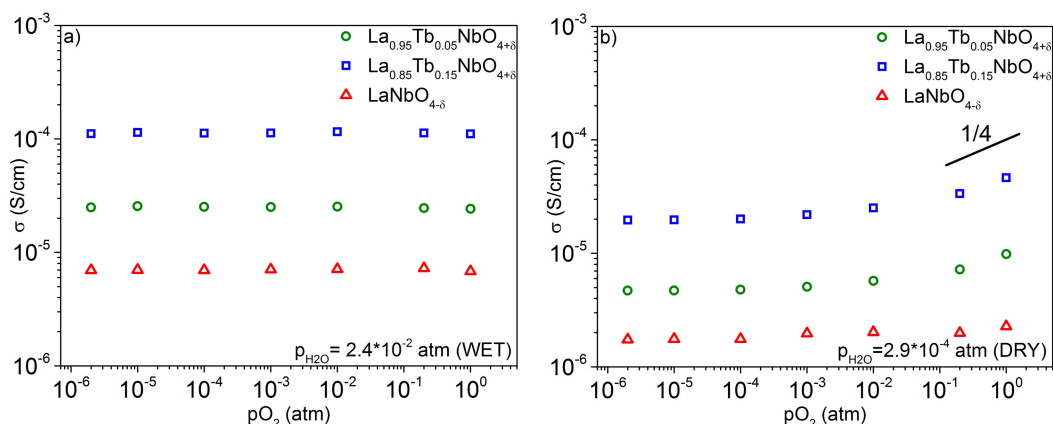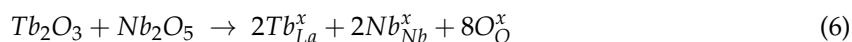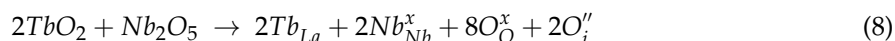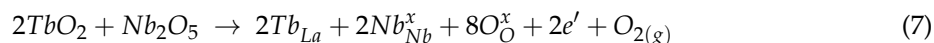

Figure 9. Total conductivity plotted as a function of pO$_2$ at 700 °C of LaNbO$_{4-\delta}$, La$_{0.05}$Tb$_{0.05}$NbO$_{4+\delta}$, and La$_{0.15}$Tb$_{0.85}$NbO$_{4+\delta}$ under (**a**) wet and (**b**) dry conditions.

The influence of Tb on the electrical properties of the material should be analyzed in view of two possible terbium oxidation states—terbium can be either isovalent (Tb^{3+}) with lanthanum (La^{3+}) or have higher oxidation state (Tb^{4+}) and serve as a donor. The source of terbium during the synthesis was Tb$_4$O$_7$, which contains a mixture of Tb^{3+} and Tb^{4+}. For simplicity in defect chemistry analysis, we will treat that oxide as a mixture of Tb$_2$O$_3$ and TbO$_2$. In the case of Tb$_2$O$_3$, in which terbium is isovalent with lanthanum, the incorporation of Tb follows the reaction (6).

$$Tb_2O_3 + Nb_2O_5 \rightarrow 2Tb_{La}^x + 2Nb_{Nb}^x + 8O_O^x \tag{6}$$

In the case of TbO$_2$, the excess positive charge of Tb^{4+} can be compensated by the formation of either electron or oxygen interstitials, which is described by reactions (7) and (8).

$$2TbO_2 + Nb_2O_5 \rightarrow 2Tb_{La} + 2Nb_{Nb}^x + 8O_O^x + 2e' + O_{2(g)} \tag{7}$$

$$2TbO_2 + Nb_2O_5 \rightarrow 2Tb_{La} + 2Nb_{Nb}^x + 8O_O^x + 2O_i'' \tag{8}$$

Another point to analyze is the preferred oxidation state of terbium in the crystal lattice of lanthanum orthoniobate. One can assume that the more preferred oxidation state of terbium is 3+, since the ionic radii difference between Tb^{3+} and La^{3+} is much smaller (0.12 Å) than that between Tb^{4+} and La^{3+} (0.28 Å). The structure with Tb^{3+} would be much less strained than with Tb^{4+}. Therefore, it may be expected that Tb^{4+} will be at least partially reduced into Tb^{3+}, which is accompanied by the generation of holes:

$$Tb_{La} \leftrightarrow Tb_{La}^x + h \tag{9}$$

Further analysis of the possible scenarios must be performed in relation to the knowledge of properties of undoped lanthanum orthoniobate. First of all, the most energetically favourable intrinsic defect in LaNbO$_{4-\delta}$ is an anion Frenkel pair, which is a pair of oxygen vacancy and oxygen interstitial [39]:

$$O_O^X \rightarrow O_i'' + V_O^{\bullet\bullet} \tag{10}$$

This indicates that the formation of interstitial oxygen ions' defects could be energetically preferred in the case of doped lanthanum niobate. Secondly, studies of LaNbO$_{4-\delta}$ [13] showed that in oxidizing conditions at 1200 °C, the material is a mixed electron hole and oxygen ion conductor. The electron holes are a minority defect (concentration-wise), however, due to the higher mobility of holes in the valence band in comparison to the mobility of ionic defects in the lattice, the overall effect is a

mixed type of conductivity. The results for lower temperatures are not presented in the study by Haugsrud et al. [13], however by the studies of similar systems [38] it can be expected that with lowering temperature the contribution from holes diminishes and for temperatures of interest in our study, doped lanthanum orthoniobate should be an oxygen ion conductor in dry conditions. Indeed, our measurement of conductivity of lanthanum orthoniobate as a function of oxygen partial pressure shows that at 700 °C at lower p_{O2} it is an ion conductor, with increasing hole contribution at higher p_{O2}. The situation is the same for Tb doped lanthanum orthoniobates. This shows similarity of properties of Tb doped samples to the pure $LaNbO_4$.

The effect of Tb substitution given by reactions (7–9) could be twofold. In the first scenario it can be either that the incorporation of Tb^{4+} produces electrons (7), and then latter partial reduction to Tb^{3+} reduces that effect by either producing holes in the reaction (9), which can further recombine with electrons. The second scenario would be the creation of oxygen interstitials (8) accompanied by the formation of holes during a partial reduction of Tb to fit into the $LaNbO_{4-\delta}$ lattice (9). The latter hypothesis of the preferred formation of oxygen interstitials instead of electrons is supported by the results of the measurement of conductivity as a function of oxygen partial pressure in dry conditions. Moreover, a similar compound, $CeNbO_{4+\delta}$, is an oxygen ion conductor, in which oxygen interstitials dominate [40]. $CeNbO_{4+\delta}$ is a compound similar to $LaNbO_{4-\delta}$. It is isostructural with $LaNbO_{4-\delta}$, but cerium occupying the A-site may be present either as Ce^{3+} or Ce^{4+}. Therefore, $CeNbO_{4+\delta}$ is expected to be somewhat similar to terbium-doped lanthanum orthoniobate because terbium doping also induces a mixed 3+/4+ oxidation state in the A-site.

All considered, an overall effect with dominating reactions (8) and (9) should be that the oxygen ionic conductivity should increase due to the formation of ionic defects and the hole contribution to total conductivity should also increase with an increase of Tb content. Indeed, the conductivity of samples with x < 0.2 increases with increasing Tb content, which means that increasing Tb content leads to the increase of the concentration of mobile charged species. This is observed both in the wet and dry atmospheres, which supports the hypothesis of dominating ionic conductivity. Moreover, conductivity measured as a function of oxygen partial pressure in wet atmospheres shows a typical feature of a proton conductor, i.e., the conductivity does not depend on the pressure. Lower conductivity observed in samples with high Tb content (x ≥ 0.2) (Figure 8) can be explained by potential trapping of ionic charged species around the dopants. This is a common feature observed in heavily doped ionic conductors [41–43].

The observed increase of the conductivity in wet air compared to dry one may be considered as a typical feature of a high-temperature proton conductor related to the hydration reaction of an oxide. Typically, the hydration reaction is given by the following:

$$H_2O + V_O^{\bullet\bullet} + O_O^x \leftrightarrow 2OH_O^\bullet \tag{11}$$

In $La_{1-x}Tb_xNbO_{4+\delta}$, however, not many vacancies are expected to be present in the system, therefore a possible alternative reaction could be given:

$$H_2O + 2O_O^X \rightarrow 2OH_O^\bullet + O_i'' \tag{12}$$

This reaction was previously proposed by Norby and discussed later by Islam for brownmillerite oxides [44,45]. Moreover, recent calculations showed oxygen ionic conductivity at high temperatures in undoped $LaNbO_4$, which may occur via oxygen interstitial positions [46]. Hydration of the doped materials may lead to the formation of both proton defects and interstitial oxygen ions. Thermogravimetric analysis showed that the mass change caused by the water uptake is rather small. The TGA results did not allow us to determine whether this depends on the terbium content. On the other hand, the analysis of the influence of the atmosphere on electrical properties shows that the relative increase of conductivity in wet atmospheres depends on the terbium content, in a similar way as the conductivity values (Table 2, Figure 7). It reaches the maximum in the $La_{0.85}Tb_{15}NbO_{4+\delta}$

sample, however, it is much lower than that in the undoped lanthanum orthoniobate—the relative change of conductivity for $LaNbO_{4-\delta}$ is 4 times higher than that for $La_{0.85}Tb_{15}NbO_{4+\delta}$. The proposed hypothesis, in which Tb presence increases the concentrations of oxygen interstitials and electron holes, could explain this observation. The hole conductivity occurs as a result of the partial reduction of Tb^{4+} in the lattice (reaction (9)), and this should not be affected by the hydration reactions (11) and (12). Therefore, with increasing terbium content, the hole conductivity also increases and the relative contribution of protons into the total conductivity should decrease.

Figure 10 presents the temperature dependence of the two components of the total conductivity, specific grain boundary, and grain interior (bulk) conductivities for $La_{0.9}Tb_{0.1}NbO_{4+\delta}$ sample, which is representative of the whole system. In the temperature range above 500 °C, the specific grain boundary conductivity is higher by over an order of magnitude than the bulk one. This is not typical behavior of solid electrolytes, however, similar phenomena were observed for $LaNbO_{4-\delta}$ co-doped with 10% praseodymium and 2% calcium [28].

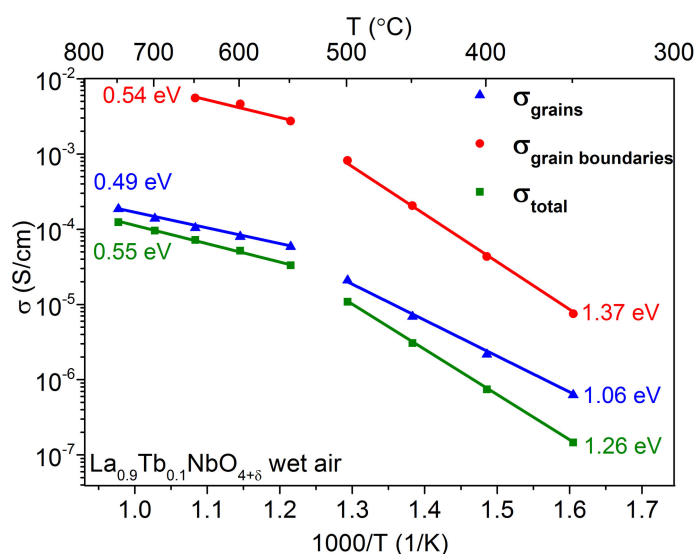**Figure 10.** Temperature dependence of total conductivity, grain conductivity, and specific grain boundary conductivity of $La_{0.9}Tb_{0.1}NbO_{4+\delta}$ measured in wet air.

4. Conclusions

Single-phase samples of terbium doped lanthanum orthoniobates were prepared and studied. Unit cell parameters at room temperature of the studied compounds were determined. A decrease of the unit cell volume with increasing terbium content was observed. The results of high-temperature XRD showed that increasing terbium content in the lanthanum sublattice causes an increase of the phase transition temperature. The phase transition temperatures were approximately 480 °C, 500 °C, and 530 °C for $La_{0.9}Tb_{0.1}NbO_{4+\delta}$, $La_{0.8}Tb_{0.2}NbO_{4+\delta}$, and $La_{0.7}Tb_{0.3}NbO_{4+\delta}$, respectively. This behavior, as well as the observed decrease of the unit cell volume with increasing terbium content, was interpreted as related to the lower ionic radius of terbium.

Temperature dependence of electrical conductivity in different atmospheres was investigated and discussed. Both terbium content and the atmosphere influence the total conductivity of $La_{1-x}Tb_xNbO_{4+\delta}$. The highest conductivity was observed for the $La_{0.85}Tb_{0.15}NbO_{4+\delta}$ sample both in dry and wet atmospheres. For all samples, the total conductivity in the wet was higher than that in the dry air. On the basis of defect formation analysis supported by the comparison with the $La_{1-x}Ce_xNbO_{4+\delta}$, the hypothesis explaining the electrical properties of $La_{1-x}Tb_xNbO_{4+\delta}$ was proposed. In particular, it was proposed that Tb presence increases the concentrations of oxygen interstitials and electron holes, whereas the hydration of the doped materials leads to the formation of both proton defects and interstitial oxygen ions, which has been confirmed by pO_2 dependency measurements. This means that

Tb increasing content and humid atmosphere lead to an increase of the concentrations of three types of charge carriers. The non-monotonic dependence of the total conductivity on terbium content was interpreted as a result of a possible defect association phenomena for high Tb contents (above 0.15).

Author Contributions: Conceptualization, K.D., M.G. and A.M.-G.; methodology, A.M.-G., K.D.,S.W., M.G.; formal analysis, M.G.; investigation, K.D., M.G.,A.M.-G.; resources, A.M.-G.; data curation, K.D., S.W., A.M.-G.; writing—original draft preparation, K.D.; writing—review and editing, M.G., S.W., A.M.-G.; supervision, M.G., A.M-G.; project administration, A.M.-G.; funding acquisition, A.M.-G.

Conflicts of Interest: The authors declare no conflict of interest.

References

1. Molenda, J.; Kupecki, J.; Baron, R.; Blesznowski, M.; Brus, G.; Brylewski, T.; Bucko, M.; Chmielowiec, J.; Cwieka, K.; Gazda, M.; et al. Status report on high temperature fuel cells in Poland—Recent advances and achievements. *Int. J. Hydrogen Energy* **2017**, *42*, 4366–4403. [CrossRef]
2. Gdula-Kasica, K.; Mielewczyk-Gryn, A.; Molin, S.; Jasinski, P.; Krupa, A.; Kusz, B.; Gazda, M. Optimization of microstructure and properties of acceptor-doped barium cerate. *Solid State Ionics* **2012**, *225*, 245–249. [CrossRef]
3. Haugsrud, R.; Norby, T. Proton conduction in rare-earth ortho-niobates and ortho-tantalates. *Nat. Mater.* **2006**, *5*, 193–196. [CrossRef]
4. Animitsa, I.; Iakovleva, A.; Belova, K. Electrical properties and water incorporation in A-site deficient perovskite $La_{1-x}Ba_xNb_3O_{9-0.5x}$. *J. Solid State Chem.* **2016**, *238*, 156–161. [CrossRef]
5. Hibino, T.; Mizutani, K.; Yajima, T.; Iwahara, H. Evaluation of proton conductivity in $SrCeO_3$, $BaCeO_3$, $CaZrO_3$ and $SrZrO_3$ by temperature programmed desorption method. *Solid State Ionics* **1992**, *57*, 303–306. [CrossRef]
6. Escolástico, S.; Vert, V.B.; Serra, J.M. Preparation and characterization of nanocrystalline mixed proton-electronic conducting materials based on the system Ln_6WO_{12}. *Chem. Mater.* **2009**, *21*, 3079–3089. [CrossRef]
7. Yajima, T.; Kazeoka, H.; Yogo, T.; Iwahara, H. Proton conduction in sintered oxides based on $CaZrO_3$. *Solid State Ionics* **1991**, *47*, 271–275. [CrossRef]
8. Sakai, T.; Isa, K.; Matsuka, M.; Kozai, T.; Okuyama, Y.; Ishihara, T.; Matsumoto, H. Electrochemical hydrogen pumps using Ba doped $LaYbO_3$ type proton conducting electrolyte. *Int. J. Hydrogen Energy* **2013**, *38*, 6842–6847. [CrossRef]
9. Haugsrud, R.; Ballesteros, B.; Lira-Cantu, M.; Norby, T. Ionic and electronic conductivity of 5% Ca-doped $GdNbO_4$. *J. Electrochem. Soc.* **2006**, *153*, J87–J90. [CrossRef]
10. Bayliss, R.D.; Pramana, S.S.; An, T.; Wei, F.; Kloc, C.L.; White, A.J.P.; Skinner, S.J.; White, T.J.; Baikie, T. Fergusonite-type $CeNbO_{4+\delta}$: Single crystal growth, symmetry revision and conductivity. *J. Solid State Chem.* **2013**, *204*, 291–297. [CrossRef]
11. Li, C.; Bayliss, R.D.; Skinner, S.J. Crystal structure and potential interstitial oxide ion conductivity of $LnNbO_4$ and $LnNb_{0.92}W_{0.08}O_{4.04}$ (Ln = La, Pr, Nd). *Solid State Ionics* **2014**, *262*, 530–535. [CrossRef]
12. Huang, H.; Wang, T.; Zhou, H.; Huang, D.; Wu, Y.; Zhou, G.; Hu, J.; Zhan, J. Luminescence, energy transfer, and up-conversion mechanisms of Yb3+and Tb3+co-doped $LaNbO_4$. *J. Alloys Compd.* **2017**, *702*, 209–215. [CrossRef]
13. Haugsrud, R.; Norby, T. High-temperature proton conductivity in acceptor-doped $LaNbO_4$. *Solid State Ionics* **2006**, *177*, 1129–1135. [CrossRef]
14. Hakimova, L.; Kasyanova, A.; Farlenkov, A.; Lyagaeva, J.; Medvedev, D.; Demin, A.; Tsiakaras, P. Effect of isovalent substitution of La^{3+} in Ca-doped $LaNbO_4$ on the thermal and electrical properties. *Ceram. Int.* **2019**, *45*, 209–215. [CrossRef]
15. Mielewczyk-Gryn, A.; Wachowski, S.; Zagórski, K.; Jasiński, P.; Gazda, M. Characterization of magnesium doped lanthanum orthoniobate synthesized by molten salt route. *Ceram. Int.* **2015**, *41*, 7847–7852. [CrossRef]
16. Mielewczyk-Gryn, A.; Gdula, K.; Lendze, T.; Kusz, B.; Gazda, M. Nano- and microcrystals of doped niobates. *Cryst. Res. Technol.* **2010**, *45*, 1225–1228. [CrossRef]

17. Fjeld, H.; Kepaptsoglou, D.M.; Haugsrud, R.; Norby, T. Charge carriers in grain boundaries of 0.5% Sr-doped LaNbO$_4$. *Solid State Ionics* **2010**, *181*, 104–109. [CrossRef]

18. Mokkelbost, T.; Lein, H.L.; Vullum, P.E.; Holmestad, R.; Grande, T.; Einarsrud, M.-A. Thermal and mechanical properties of LaNbO$_4$-based ceramics. *Ceram. Int.* **2009**, *35*, 2877–2883. [CrossRef]

19. Nguyen, D.; Kim, Y.H.; Lee, J.S.; Fisher, J.G. Structure, morphology, and electrical properties of proton conducting La$_{0.99}$Sr$_{0.01}$NbO$_{4-\delta}$ synthesized by a modified solid state reaction method. *Mater. Chem. Phys.* **2017**, *202*, 320–328. [CrossRef]

20. Brandão, A.D.; Antunes, I.; Frade, J.R.; Torre, J.; Kharton, V.V.; Fagg, D.P. Enhanced Low-Temperature Proton Conduction in Sr$_{0.02}$La$_{0.98}$NbO$_{4-\delta}$ by Scheelite Phase Retention. *Chem. Mater.* **2010**, *22*, 6673–6683. [CrossRef]

21. Wachowski, S.; Mielewczyk-Gryn, A.; Gazda, M. Effect of isovalent substitution on microstructure and phase transition of LaNb$_{1-x}$M$_x$O$_4$ (M = Sb, V or ta; x = 0.05 to 0.3). *J. Solid State Chem.* **2014**, *219*, 201–209. [CrossRef]

22. Brandão, A.D.; Nasani, N.; Yaremchenko, A.A.; Kovalevsky, A.V.; Fagg, D.P. Solid solution limits and electrical properties of scheelite SryLa$_{1-y}$Nb$_{1-x}$V$_x$O$_{4-\delta}$ materials for x = 0.25 and 0.30 as potential proton conducting ceramic electrolytes. *Int. J. Hydrogen Energy* **2018**, *43*, 18682–18690. [CrossRef]

23. Wachowski, S.; Mielewczyk-Gryn, A.; Zagorski, K.; Li, C.; Jasinski, P.; Skinner, S.J.; Haugsrud, R.; Gazda, M. Influence of Sb-substitution on ionic transport in lanthanum orthoniobates. *J. Mater. Chem. A* **2016**, *4*, 11696–11707. [CrossRef]

24. Mielewczyk-Gryn, A.; Wachowski, S.; Strychalska, J.; Zagórski, K.; Klimczuk, T.; Navrotsky, A.; Gazda, M. Heat capacities and thermodynamic properties of antimony substituted lanthanum orthoniobates. *Ceram. Int.* **2016**, *42*, 7054–7059. [CrossRef]

25. Mielewczyk-Gryn, A.; Wachowski, S.; Lilova, K.I.; Guo, X.; Gazda, M.; Navrotsky, A. Influence of antimony substitution on spontaneous strain and thermodynamic stability of lanthanum orthoniobate. *Ceram. Int.* **2015**, *41*, 2128–2133. [CrossRef]

26. Wachowski, S.; Kamecki, B.; Winiarz, P.; Dzierzgowski, K.; Mielewczyk-Gryń, A.; Gazda, M. Tailoring structural properties of lanthanum orthoniobates through an isovalent substitution on the Nb-site. *Inorg. Chem. Front.* **2018**, *5*, 2157–2166. [CrossRef]

27. Li, M.; Wu, R.; Zhu, L.; Cheng, J.; Hong, T.; Xu, C. Enhanced sinterability and conductivity of cobalt doped lanthanum niobate as electrolyte for proton-conducting solid oxide fuel cell. *Ceram. Int.* **2019**, *45*, 573–578. [CrossRef]

28. Dzierzgowski, K.; Wachowski, S.; Gojtowska, W.; Lewandowska, I.; Jasiński, P.; Gazda, M.; Mielewczyk-Gryń, A. Praseodymium substituted lanthanum orthoniobate: Electrical and structural properties. *Ceram. Int.* **2018**, *44*, 8210–8215. [CrossRef]

29. Packer, R.J.; Skinner, S.J.; Yaremchenko, A.A.; Tsipis, E.V.; Kharton, V.V.; Patrakeev, M.V.; Bakhteeva, Y.A. Lanthanum substituted CeNbO$_{4+\delta}$ scheelites: Mixed conductivity and structure at elevated temperatures. *J. Mater. Chem.* **2006**, *16*, 3503. [CrossRef]

30. Rodríguez-Carvajal, J. *Recent Developments for the Program FULLPROF*; Commission on Powder Diffraction: Perth, Australia, 2001; Volume 26, ISBN 4971168915.

31. Shannon, R.D. Revised effective ionic radii and systematic studies of interatomic distances in halides and chalcogenides. *Acta Crystallogr. Sect. A* **1976**, *32*, 751–767. [CrossRef]

32. Stubičan, V.S. High-Temperature Transitions in Rare Earth Niobates and TantaIates. *J. Am. Ceram. Soc.* **1964**, *47*, 55–58. [CrossRef]

33. Yamazaki, Y.; Babilo, P.; Haile, S.M. Defect chemistry of yttrium-doped barium zirconate: A thermodynamic analysis of water uptake. *Chem. Mater.* **2008**, *20*, 6352–6357. [CrossRef]

34. Mielewczyk-Gryń, A. Water uptake analysis of the acceptor-doped lanthanum orthoniobates. *J. Therm. Anal. Calorim.* **2019**, submitted.

35. Huse, M.; Norby, T.; Haugsrud, R. Effects of A and B site acceptor doping on hydration and proton mobility of LaNbO$_4$. *Int. J. Hydrogen Energy* **2012**, *37*, 8004–8016. [CrossRef]

36. Abrantes, J.C.C.; Labrincha, J.A.; Frade, J.R. Applicability of the brick layer model to describe the grain boundary properties of strontium titanate ceramics. *J. Eur. Ceram. Soc.* **2000**, *20*, 1603–1609. [CrossRef]

37. Haile, S.M.; West, D.L.; Campbell, J. The role of microstructure and processing on the proton conducting properties of gadolinium-doped barium cerate. *J. Mater. Res.* **1998**, *13*, 1576–1595. [CrossRef]

38.	Berger, P.; Mauvy, F.; Grenier, J.-C.; Sata, N.; Magrasó, A.; Haugsrud, R.; Slater, P.R. *Proton-Conducting Ceramics: From Fundamentals to Applied Research*; Marrony, M., Ed.; Pan Stanford Publishing: Singapore, 2016; Chapter 1; pp. 1–72.

39.	Mather, G.C.; Fisher, C.A.J.; Islam, M.S. Defects, dopants, and protons in LaNbO$_4$. *Chem. Mater.* **2010**, *22*, 5912–5917. [CrossRef]

40.	Packer, R.J.; Tsipis, E.V.; Munnings, C.N.; Kharton, V.V.; Skinner, S.J.; Frade, J.R. Diffusion and conductivity properties of cerium niobate. *Solid State Ionics* **2006**, *177*, 2059–2064. [CrossRef]

41.	Wang, D.Y.; Park, D.S.; Griffith, J.; Nowick, A.S. Oxygen-ion conductivity and defect interactions in yttria-doped ceria. *Solid State Ionics* **1981**, *2*, 95–105. [CrossRef]

42.	Guo, X.; Waser, R. Electrical properties of the grain boundaries of oxygen ion conductors: Acceptor-doped zirconia and ceria. *Prog. Mater. Sci.* **2006**, *51*, 151–210. [CrossRef]

43.	Kilner, J.A.; Brook, R.J. A study of oxygen ion conductivity in doped non-stoichiometric oxides. *Solid State Ionics* **1982**, *6*, 237–252. [CrossRef]

44.	Norby, T.; Larring, Y. Concentration and transport of protons in oxides. *Curr. Opin. Solid State Mater. Sci.* **1997**, *2*, 593–599. [CrossRef]

45.	Islam, M.S.; Davies, R.A.; Fisher, C.A.J.; Chadwick, A.V. Defects and protons in the CaZrO$_3$ perovskite and Ba$_2$In$_2$O$_5$ brownmillerite: Computer modelling and EXAFS studies. *Solid State Ionics* **2001**, *145*, 333–338. [CrossRef]

46.	Toyoura, K.; Sakakibara, Y.; Yokoi, T.; Nakamura, A.; Matsunaga, K. Oxide-ion conduction: Via interstitials in scheelite-type LaNbO$_4$: A first-principles study. *J. Mater. Chem. A* **2018**, *6*, 12004–12011. [CrossRef]